Density functional theory examination of Pd(111) and Pd(100) under NO oxidation conditions

Jelena Jelic and Randall J. Meyer
Department of Chemical Engineering, University of Illinois at Chicago, 810 S. Clinton, Chicago, Illinois 60607, USA
(Received 18 July 2008; revised manuscript received 27 October 2008; published 6 March 2009)

We have used density functional theory calculations combined with a thermodynamic analysis to investigate the composition and structure of Pd(100) and Pd(111) surfaces for NO oxidation over a wide range of temperatures and pressures. Results indicate that unlike the case for CO oxidation, the bulk oxide is the thermodynamically favored phase over large regions in the phase diagram for both surfaces of palladium. At the conditions for NO oxidation in the NO_x storage reduction cycle, the surface is expected to be the clean PdO(101) surface, although kinetic limitations may exist.

DOI: 10.1103/PhysRevB.79.125410 PACS number(s): 82.45.Jn

I. INTRODUCTION

Lean NO_x Traps or NO_x storage reduction (NSR) systems[1–3] have been a subject of considerable attention recently as the need for more fuel efficient engines is exacerbated by rising fuel prices. NSR catalysts are typically composed of at least one alkali or alkaline-earth component and at least one precious-metal component, which are supported on a high surface area refractory oxide. The most common catalyst formulation includes platinum as the metal component which is required to perform the demanding task of acting as both an oxidation catalyst and as a reduction catalyst operating in two distinct modes. Recent studies from Harold and Amiridis[4] indicate that performance at low temperature could be possibly improved by switching to palladium. A key to better performance in this catalyst is the improved efficiency of the NO oxidation reaction. Previously, Ovesson and co-workers[5,6] have examined this reaction in great detail over Pt(111). One important conclusion from Schneider's work is that the oxygen surface coverage is likely to be high under reaction conditions.

As has been shown both experimentally in the work of Hendriksen and co-workers[7,8] and theoretically by Reuter and co-workers,[9–11] under realistic operating conditions, in heterogeneous oxidation catalysts, the active surface for catalysis may actually be a surface oxide instead of a pristine metal surface. Using the concept of *ab initio* thermodynamics, whereby density functional theory (DFT) calculations of surfaces are used in concert with free-energy relationships, Reuter and Scheffler have published extensively on this subject with their examination of CO oxidation for various metals including Pd.[11–16] In this case, CO oxidation may occur on the surface oxide. However, Goodman's work has recently suggested that the rate greatly increases when the oxygen and CO pressures are held such that the surface has not fully converted to the oxide (but may actually be in the midst of a phase transformation).[17] In an effort to mimic the results of Reuter and Scheffler and obtain quantitative atomic-scale insight we examine a variety of surface structures and compositions on both Pd(100) and Pd(111) when exposed to a reactive gas atmosphere consisting of O_2 and NO (to replicate the gas environment for NSR catalysts).

II. COMPUTATIONAL METHODOLOGY

The density functional theory calculations in this work are performed using the Vienna *Ab Initio* Simulation Package (VASP).[18,19] A plane-wave basis set with a cutoff energy of 400 eV and ultrasoft Vanderbilt pseudopotentials (U.S.-PP) (Ref. 20) were employed. The Perdew Wang (PW-91) form of the generalized gradient approximation (GGA) (Ref. 21) exchange and correlation functional was used in all calculations reported herein.

All the calculations were done for "mirror" surfaces, with adsorbates on both sides and at least 12 Å of vacuum between surfaces. For all systems, except for the surface oxide formed on Pd(111), we used five layer thick metal slabs. Three middle layers of metal were held fixed while the top metal layers, adsorbates, and oxide layer were relaxed.

Different unit cells were used to represent the different surface structures depending on the adsorbate coverage. For adsorption on the Pd(100) and Pd(111) surfaces and systems with $p(2\times2)$ and $c(2\times2)$ coverages of both adsorbates, a small unit cell (2×2) is used with Brillouin-zone sampling in a uniform $7\times7\times1$ *k*-point grid (Monkhorst-Pack).[22] For systems with bigger unit cells [$c(4\times2)$, $c(6\times2)$ and similar] the Brillouin zone is sampled with a uniform $5\times5\times1$ *k*-point grid. Structures were converged with regard to both *k* points and cutoff energies to within 0.02 eV/adsorbate atom (O or NO).

A surface oxide with a $(\sqrt{5}\times\sqrt{5})R27°$ structure has been observed to form on Pd(100),[23,24] which corresponds to a subnanometer thin film of PdO(101) on the metal surface. In this case a single stoichiometric layer is modeled above the metal slab with the top metal layer and oxide layer allowed to relax. The Brillouin zone was sampled with $5\times5\times1$ *k*-point grid (Monkhorst-Pack).

The surface oxide formed on Pd(111) surface corresponds to a Pd_5O_4 structure.[25] The smallest unit cell of the underlying metal that could be made to match with oxide layer was 4×12. For this system only three layers of palladium were used. The middle layer of the metal oxide/metal sandwich was fixed, while the top metal layer and the oxide layer were relaxed. The Brillouin zone is sampled using a gamma point (single *k* point) calculation due to its large size. Due to the size of the unit cells for the surface oxides, we did not perform convergence tests with regard to cell size or thickness.

To determine the energy of bulk Pd, a four atom fcc unit cell was used (with a dense $13\times13\times13$ *k*-point grid) whose atomic positions were optimized resulting in a slightly expanded lattice constant (3.96 Å) with respect to experimental values (3.89 Å). Finally, the energies of all molecules (NO, O_2 etc.) were calculated using a single molecule in a 10 Å cube with gamma point sampling.

III. RESULTS AND DISCUSSION

Our analysis of the surface termination follows the methodology of Scheffler and co-workers.[9–16,26–28] This approach relies on the principle that the surface with the lowest surface energy will be the observed termination for a given thermodynamic (T, P) condition. Neglecting kinetic effects of catalytic reactions on the surface structure, the surface is considered to be in equilibrium with i separate reservoirs representing the i gas phase species (in this case two: NO and O_2), each characterized by partial pressure p_i and temperature T (or chemical potential $\Delta\mu_i(T,p_i)$ summarizing this two-dimensional dependences).

The thermodynamically favored surface will have the lowest surface energy, Ω,

$$\Omega = \frac{1}{2A}\left[G_{\text{slab}}^{\text{surf}}(T,N_i,P_i) - \sum_i N_i\mu_i(T,p_i)\right]. \quad (1)$$

The surface free energy is normalized to the energy per surface area by dividing it by the area of the surface unit cell, A, accounting for the two equivalent surfaces of the slab.

The Gibbs free energies of the solid phase, G_{slab} can be decomposed into the contributing terms,

$$G = E^{\text{TOTAL}} + F^{\text{vib}} - TS^{\text{conf}} + pV, \quad (2)$$

where E^{TOTAL} is the total energy, excluding the zero-point energy, F^{vib} is the vibrational free energy and S^{conf} is the configurational entropy.

From Eq. (1) (Ref. 10) it is obvious that the surface free energy depends on differences in the Gibbs free energies of the slab and the bulk metal and it can be expressed as $\Delta G = \Delta E^{\text{TOTAL}} + \Delta F^{\text{vib}} - T\Delta S^{\text{conf}} + \Delta(pV)$. For solid systems, $\Delta(pV)$ term is negligibly small. The vibrational free-energy component can be determined by calculating the vibrational frequencies of all the bonds in the system. For example, the calculated vibrational frequency of adsorbed oxygen is 472 cm^{-1} for 0.25 ML coverage and the calculated frequency for adsorbed NO is 1549 cm^{-1} for the same coverage on Pd(111) surface at the fcc threefold hollow sites. Following the procedure of Reuter and Scheffler,[26] we have calculated that the vibrational free-energy contribution from the various surfaces ranges from 2–5 $\text{meV}/\text{Å}^2$ for the temperatures up to 700 K. Configurational entropy was calculated following the method given by Reuter and Scheffler.[10] This entropic contribution is also small: a maximum of 5 $\text{meV}/\text{Å}^2$ for the temperatures up to 700 K. Therefore given the magnitudes of the $\Delta(pV)$, ΔF^{vib}, and $T\Delta S^{\text{conf}}$ contributions, we can safely neglect these terms.

Including all this approximations we are left with $\Delta G = \Delta E^{\text{TOTAL}}$, where E^{TOTAL}'s are the DFT calculated energies. Therefore we can rewrite Eq. (1) as

$$\Omega = \frac{1}{2A}\left(E^{\text{TOTAL}} - \sum N\mu\right), \quad (3)$$

where the chemical potential of gas phase species are determined by

TABLE I. Calculated adsorption energies (eV) of O (per atom) and NO (per molecule) on Pd(100).

Oxygen structures	Coverage	E^{bind}
$p(2\times2)$-f	0.25	−1.23
$c(2\times2)$-f	0.50	−1.05
NO structures		
$(\sqrt{3}\times\sqrt{3})$ bridge	0.33	−2.14
$c(2\sqrt{2}\times\sqrt{2})$ bridge	0.50	−2.10
$c(2\times2)$ bridge	0.50	−2.00
$p(1\times1)$ bridge	1.00	−1.51

$$\mu(T,P) = \Delta H(T,P^\circ) + E_{\text{gas}} - T\Delta S(T,P^\circ) + k_B T\ln(P/P^\circ), \quad (4)$$

E^{TOTAL} and E_{gas} are calculated DFT energies (E^{TOTAL} is the energy of slab with adsorbates and E_{gas} is energy of gas phase molecule—NO or O_2), while ΔH and ΔS terms (enthalpy and entropy of gas phase molecules formation) were taken from thermodynamic tables (although these can be determined from our DFT calculations as well).[29] The chemical potential of a bulk Pd atom is equal to the Gibbs free energy (or in this case, its calculated energy from DFT given our previous approximations for the free energy of the slab).

Within this approach we are then in a position to compare the stability of a wide range of possible surface structural models under various conditions (T, p_{O_2}, p_{NO}) ranging from ultrahigh vacuum to atmospheric pressures at any temperature. Many possible surface structure configurations were examined for both Pd(100) and Pd(111), but only a few of them were found to be most stable in the range of O_2 and NO chemical potentials examined.

First, we have calculated the adsorption energies of both O_2 and NO on Pd(100) and Pd(111). When Pd(100) surface is exposed to oxygen, three well established surfaces have been observed experimentally and well characterized: $p(2\times2)$ at 0.25 ML, $c(2\times2)$ at 0.5 ML and the $(\sqrt{5}\times\sqrt{5})R27°$—surface oxide.[30,31] In agreement with previous results, we have calculated the adsorption of oxygen for each of these surfaces and find that for both $p(2\times2)$ and $c(2\times2)$ structures, the fourfold hollow site is the most stable one.[30,32] Calculated adsorption energies reported with respect to the O_2 gas phase molecule for thermodynamically favorable configurations are given in Table I (structures are shown in Fig. 1). There is an expected decrease in adsorption energies with increase in coverage because of the repulsion between adsorbed O atoms.[33] The binding energy of oxygen (referenced to gas phase O_2) within the surface oxide is −1.14 eV.

Similar structures are observed for O_2 adsorption on Pd(111): $p(2\times2)$, $c(2\times2)$ and the Pd_5O_4 surface oxide.[23] The most favorable adsorption site for both the 0.25 and 0.50 ML coverages is the fcc threefold hollow site.[34,35] For 0.50 ML we have found that the $p(2\times2)-f+h$ structure (fcc hollow site+hcp hollow site) is less favorable than $c(2\times2)-f$. Adsorption energies are given in Table II (structures are

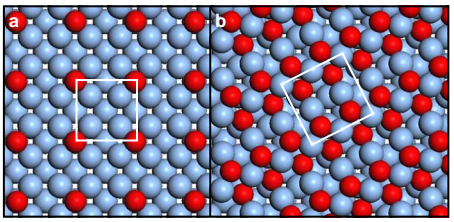

FIG. 1. (Color online) Top view of thermodynamically favorable surfaces for oxygen adsorption on Pd(100); (a) $p(2\times2)-f$, representing 0.25 ML coverage and (b) PdO(101) surface oxide over Pd(100). Oxygen atoms are shown in red (dark gray). Palladium atoms are metallic blue (light gray).

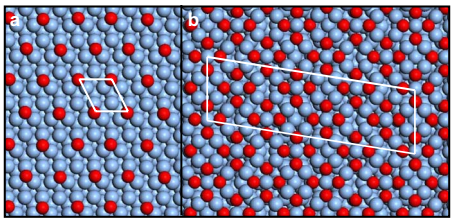

FIG. 2. (Color online) Top view of thermodynamically favorable surfaces for oxygen adsorption on Pd(111); (a) $p(2\times2)-f$, representing 0.25 ML coverage and (b) Pd_5O_4, surface oxide on Pd(111).

shown in Fig. 2). Once again, increasing the coverage leads to a decrease in adsorption energy. The binding energy of oxygen within the Pd_5O_4 surface oxide is −1.08 eV, slightly less than on the PdO(101) surface.

Various coverages for NO adsorption on both surfaces have been examined as well. For Pd(100), two structures have been experimentally observed, $c(4\times2)$ and $c(2\sqrt{2}\times\sqrt{2})$.[36] For $c(2\sqrt{2}\times\sqrt{2})$ structure, the fourfold hollow site is the most favorable adsorption site and for $c(4\times2)$, the bridge site is favored. A combined low-energy electron diffraction (LEED) and electron-energy-loss spectroscopy (EELS) study of NO adsorption on Pd(100) revealed that at low coverage (0.25 ML) NO adsorbs at the fourfold hollow site, while at higher coverages, the bridge site is preferred.[36,37] Our calculations show that for 0.25 ML of NO the adsorption energies of these two sites are isoenergetic (E_{ads}=−2.16 eV for fourfold hollow site and E_{ads} =−2.15 eV for bridge site). At higher coverage, this remains the case (E_{ads}=−1.96 eV for the $c(2\times2)$ fourfold hollow site compared to −2.00 eV for the $c(2\times2)$ bridge site). We have calculated the adsorption energies for these two structures as well as additional possible structures on Pd(100) [such as $p(2\times2)$, $(\sqrt{3}\times\sqrt{3})$, $c(2\times2)$, $c(6\times2)$, $c(8\times2)$, $p(1\times1)$]. NO adsorption energies for thermodynamically favorable surfaces are given in Table I (structures are depicted in Fig. 3). As expected, the adsorption energy decreases with increase in coverage.

For Pd(111),[38,39] the most favorable adsorption site at low coverage (≤0.33 ML) for NO is the fcc threefold follow site in agreement with previous experimental studies.[40,41] As coverage increases, the preferred adsorption site changes such that the hcp threefold hollow site is filled at 0.50 ML. Finally at 0.75 ML NO, the atop or t/t (tilting atop) site is occupied. Adsorption energies for the favorable adlayer structures as shown in the phase diagram (Fig. 6) are given in Table II and shown in Fig. 4.

TABLE II. Calculated adsorption energies (eV) of O (per atom) and NO (per molecule) on Pd(111).

Oxygen structures	Coverage	E^{bind}
$p(2\times2)$-f	0.25	−1.31
$c(2\times2)$-f+h	0.50	−1.01
NO structures		
$c(6\times2)$-f	0.17	−2.35
$(\sqrt{3}\times\sqrt{3})$-f	0.33	−2.28
$c(4\times2)$-f+h	0.50	−2.10
$p(2\times2)$-f+h+t/t	0.75	−1.71

Atomic oxygen adsorbs quite weakly on both the Pd_5O_4 and PdO(101) surface oxides. Adsorption energies (per oxygen atom reference to O_2) for oxygen on the Pd_5O_4 oxide are: −0.16 eV for 0.15 ML coverage (fourfold hollow adsorption site), −0.11 eV for 0.29 ML coverage (fourfold plus bridge sites) and at 0.44 ML coverage, adsorption is thermoneutral (+0.01 eV). On the PdO(101) surface oxide, oxygen adsorbs at the bridge site between two threefold coordinated Pd atoms with −0.03 eV at 0.20 ML coverage and adsorption becomes endothermic at 0.40 ML coverage (0.19 eV). Hinojosa *et al.*[42] have recently examined O_2 adsorption on thin Pd films. Temperature programmed desorption experiments indicate the presence of weakly bound molecular oxygen (at 117 K and 227 K) with a saturation coverage of 0.27 ML at 85 K on PdO(101). Isotope experiments confirm that O_2 did not dissociate on this surface. In contrast, O_2 did not adsorb on Pd_5O_4/Pd(111). Our calculations also show that molecular rather than atomic oxygen is thermodynamically favorable, as O_2 weakly adsorbs at the hollow site (−0.28 eV) between three- and fourfold coordinated Pd on PdO(101) (shown in Fig. 7), but with a similar result for the Pd_5O_4 oxide surface (−0.25 eV).

NO adsorbs more strongly to both surface oxides as compared to oxygen. On the Pd_5O_4 oxide, at 0.15 ML coverage (fourfold hollow site) the adsorption energy per NO mol-

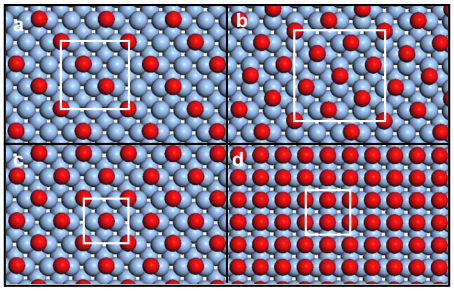

FIG. 3. (Color online) Top view of thermodynamically favorable surfaces for NO adsorption on Pd(100); (a) $(\sqrt{3}\times\sqrt{3})$ *bridge*, representing 0.33 ML coverage, (b) $c(2\sqrt{2}\times\sqrt{2})$ *bridge*, with 0.5 ML coverage, (c) $c(2\times2)$ *bridge*, with 0.5 ML coverage, and (d) $p(1\times1)$ *bridge*, with 1.0 ML coverage.

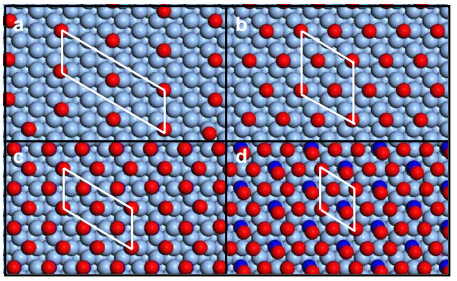

FIG. 4. (Color online) Top view of thermodynamically favorable surfaces for NO adsorption on Pd(111); (a) $c(6\times2)-f$, with 0.17 ML coverage, (b) $(\sqrt{3}\times\sqrt{3})-f$, with 0.33 ML coverage, (c)$(4\times2)-f+h$, with 0.5 ML coverage, and (d) $p(2x2)-f+h+t/t$, with 0.75 ML coverage.

ecule is −1.08 eV. On the PdO(101) oxide, at 0.20 ML coverage (bridge site between threefold coordinated Pd atoms) the adsorption energy of NO is −1.12 eV (shown in Fig. 7).

Using the calculated energy, given in Eq. (3), we now construct phase diagrams which summarize the stability regions in $\Delta\mu_O$, $\Delta\mu_{NO}$ coordinates for Pd(100) (Fig. 5) and Pd(111) (Fig. 6) at $T=600$ K. From the calculations described above, we have determined the surface energies of our various models and our phase diagram is constructed by an examination of the lowest energy surface for a given T and P condition. As indicated, we have arbitrarily chosen a temperature of 600 K (designed to correspond to an average condition for emissions control catalysis). However, changing the temperature merely has the effect of sliding the pressure scale. (For the same chemical potential, increasing the temperature requires a higher pressure.)

The bottom left part of both Figs. 5 and 6 corresponds to the region of vanishing concentrations of gas phase species so the clean Pd(100) and Pd(111) surfaces result as the most stable system states. Moving from this point to the right, i.e., increasing the O_2 pressure while keeping the NO pressure low, we find surface structures containing an increasing amount of oxygen. For Pd(111), the first stable ordered structure is $p(2\times2)-f$ O, which corresponds to a coverage of θ

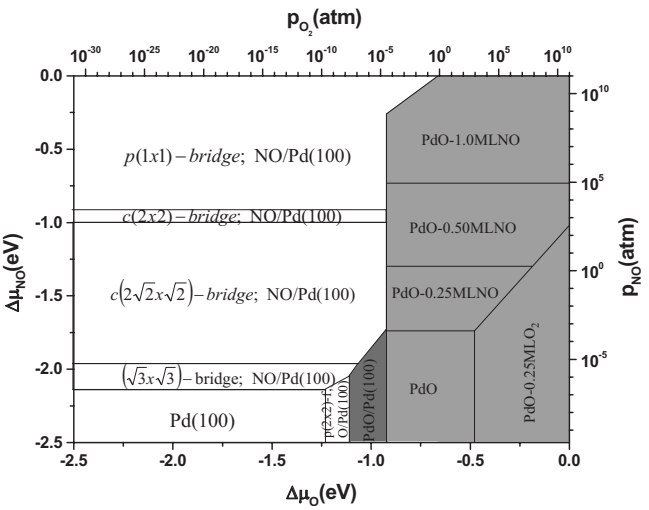

FIG. 5. Phase diagram for Pd(100) system at $T=600$ K.

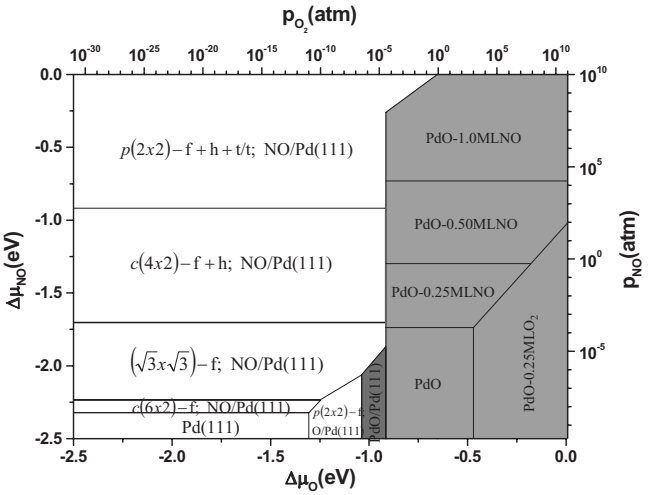

FIG. 6. Phase diagram for Pd(111) system at $T=600$ K.

=0.25 monolayer with O atoms adsorbed at the fcc threefold hollow sites. A similar type of structure $p(2\times2)$-bridge O is formed on Pd(100). The first adlayer structure formed on Pd(100) is at $\Delta\mu_O=-1.23$ eV and on Pd(111) is at $\Delta\mu_O=-1.31$ eV.

While further increasing the O_2 pressure and keeping NO pressure low, surface oxide structures are predicted to form. Rewriting Eq. (3), the Gibbs free energy for the surface oxide over a metal substrate is calculated in the same way as any adlayer structure,

$$\Omega = \frac{1}{2A}(E^{\mathrm{TOTAL}} - N_{\mathrm{Pd}}E^{\mathrm{bulk}}_{\mathrm{Pd}} - N_{\mathrm{O}}\mu_{\mathrm{O}} - N_{\mathrm{NO}}\mu_{\mathrm{NO}}), \quad (5)$$

E^{TOTAL} is the DFT calculated energy of surface oxide over Pd(100) or Pd(111) and $E^{\mathrm{bulk}}_{\mathrm{Pd}}$ is DFT calculated energy of bulk Pd.

When the O_2 pressure is kept very low and the NO pressure is increased, a series of ordered NO adsorption phases on Pd(100) and Pd(111) are predicted to be the lowest energy surfaces in good agreement with experiment.[36,39] As in the case of oxygen adsorption, NO adsorbs more strongly on Pd(111) when compared to adsorption on Pd(100) at low coverage, so the first adlayer NO structure is formed on Pd(111) at a lower chemical potential of NO than on Pd(100). The bottom right corner in both phase diagrams is the region where the bulk oxide structure is stable.[14]

In a pure oxygen environment μ_O variations may be restricted to a finite range. Below the so-called "oxygen poor limit" the oxide will decompose into Pd metal and oxygen, i.e., the oxide is only stable if

$$E^{\mathrm{bulk}}_{\mathrm{PdO}} < E^{\mathrm{bulk}}_{\mathrm{Pd}} + \mu_{\mathrm{O}}, \quad (6)$$

or in an alternate formulation if

$$\Delta\mu_{\mathrm{O}} > E^{\mathrm{bulk}}_{\mathrm{PdO}} - E^{\mathrm{bulk}}_{\mathrm{Pd}} - \frac{1}{2}E^{\mathrm{TOTAL}}_{\mathrm{O_2}}, \quad (7)$$

where $E^{\mathrm{TOTAL}}_{\mathrm{O_2}}$ is DFT calculated energy of O_2 molecule in vacuum and

$$\Delta\mu_O = \mu_O - \frac{1}{2}E_{O_2}^{TOTAL}. \quad (8)$$

The "O-rich limit" refers to conditions where oxygen will condense and this gives our second restriction,

$$\Delta\mu_O < 0. \quad (9)$$

Furthermore, the bulk oxide PdO can also be destroyed (reduced) by NO. In a pure NO environment, the stability condition for the oxide is

$$E_{PdO}^{bulk} + \mu_{NO} < E_{Pd}^{bulk} + \mu_{NO_2}. \quad (10)$$

During the oxidation cycle of NSR catalysis, NO_2 is formed by catalytic NO oxidation on the surface. However, the gas phase reaction of NO and O_2 can also occur. In our constrained equilibrium approach, we have ignored the contribution to NO_2 formation by gas phase reactions. In addition, it is assumed that the probability of NO_2 readsorption is very low compared to O_2 and NO adsorption. However, unlike the case of CO oxidation where this assumption about product (CO_2) readsorption is most certainly valid, this may not be true for NO oxidation. In the current work, we will not address this point. However, it deserves mentioning that in recent work from Schneider and Getman,[43] a phase diagram has been expressed in terms of the NO/NO_2 ratio, an alternative representation which accounts for the possibility (probability) of NO_2 readsorption. Schneider and co-workers[6] have suggested that the surface coverage at high oxygen pressures (and high NO pressures) on Pt(111) will result facile NO_2 formation and that NO_2 dissociation on the surface can lead to even higher O coverages than that predicted by O_2 alone. Following Scheffler and Reuter's[10,11] work on CO oxidation, in our formulation where the surface does not equilibrate with gas phase NO_2, the simplest way to estimate NO_2 free energy is to use the total energy of free NO_2 molecule

$$\mu_{NO_2} = E_{NO_2}^{TOTAL}. \quad (11)$$

We can express $E_{NO_2}^{TOTAL}$ with the zero Kelvin free energies of the NO_2, NO, and O_2 gas phase molecules. The stability condition for bulk palladium oxide in NO environment is

$$\Delta\mu_{NO} < -E_{PdO}^{bulk} + E_{Pd}^{bulk} + \frac{1}{2}E_{O_2}^{TOTAL} + E_{NO_2}^{bind} - E_{NO}^{bind} - \frac{1}{2}E_{O_2}^{bind}, \quad (12)$$

where

$$\Delta\mu_{NO} = \mu_{NO} - E_{NO}^{TOTAL}. \quad (13)$$

E_{NO}^{TOTAL} is DFT calculated energy of NO molecule in vacuum.

Binding energies of gas phase molecules are defined as

$$E_{x_n y_m}^{bind} = E_{x_n y_m}^{TOTAL} - nE_x^{TOTAL} - mE_y^{TOTAL}. \quad (14)$$

From our DFT calculations, $NO_2^{bind} = -10.75$ eV, $NO^{bind} = -6.74$ eV and $O_2^{bind} = -5.63$ eV. Note that the O_2 binding energy is −5.63 eV, somewhat greater than the experimental value.[44] A recent study by Hellman *et al.*[45] suggests that despite the large error associated with the oxygen binding energy, NO oxidation is well described by DFT.

For the pure O_2 regime, the stability condition for bulk PdO is: $\Delta\mu_O < -0.92$ eV. This implies that if the oxygen chemical potential is lower than −0.92 eV, bulk PdO is no longer stable and will decompose to Pd metal and gas phase O_2.

In the pure NO regime, the stability condition for bulk PdO is: $\Delta\mu_{NO} > -0.26$ eV. Consequently, if the chemical potential of NO is high enough, NO will react with oxygen from bulk PdO to form a NO_2 molecule and bulk PdO will be destroyed.

If O_2 and NO are both present in the gas phase, we will consider that PdO is in thermodynamic equilibrium with O_2 and NO individually, while O_2 and NO in the gas phase are not equilibrated.

$$\Delta\mu_{NO} - \Delta\mu_O < -2^*\left(E_{PdO}^{bulk} - E_{Pd}^{bulk} - \frac{1}{2}E_{O_2}^{total}\right) + E_{NO_2}^{bind} - E_{NO}^{bind} - \frac{1}{2}E_{O_2}^{bind}. \quad (15)$$

Therefore, the region of bulk oxide is defined such that the sum of $\Delta\mu_{NO} - \Delta\mu_O \leq 0.66$ eV.

We have also examined the possible adsorption structures of oxygen and NO on bulk PdO(101) since this termination is likely to form as oxidation of the bulk proceeds even on Pd(111).[46] Rewriting Eq. (5), the Gibbs free energy for the PdO(101) is calculated as

$$\Omega = \frac{1}{2A}(E^{TOTAL} - N_{PdO}E_{PdO}^{bulk} - N_O\mu_O - N_{NO}\mu_{NO}), \quad (16)$$

where E^{TOTAL} is the DFT calculated energy of PdO(101) slab with adsorbents, and E_{PdO}^{bulk} is DFT calculated energy of bulk PdO.

If the NO pressure is held below 10^{-3} bar, the pristine PdO(101) surface will be stable till almost 10^6 atm of oxygen (at 600 K). Above this pressure, the bulk oxide with 0.25 ML of molecular oxygen will be the most stable surface. As the NO pressure is increased, the structure that first appears as a thermodynamically stable surface will be that with 0.25 ML of NO (the structure with 0.16 ML of NO will be stable in such a short range of NO chemical potential (-1.70 eV $< \Delta\mu < -1.65$ eV) that it is not presented on our phase diagram). With an additional increase in the NO pressure, a 0.50 ML NO/PdO(101) structure will be stable (NO at both threefold Pd bridge sites) and at extremely high pressure a full monolayer of NO will condense on PdO(101) (bridge, fourfold Pd atop). All these structures are shown in Fig. 7.

It is interesting to mention that if we have very high coverage of oxygen 0.50 ML and 0.25 ML of NO on PdO(101) surface, formation of NO_2 molecule will occur spontaneously. Also, at 0.75 ML O and 0.25 ML of NO, NO_2 and O_2 will form spontaneously. These surfaces, however, are not lowest surface energy configurations for any combination of NO and O chemical potentials.

It is interesting to compare the stability of bulk PdO under CO and NO oxidation conditions. Naturally, $\Delta\mu_O$, at the

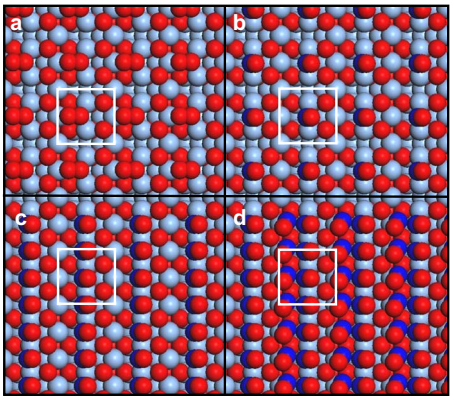

FIG. 7. (Color online) Top view of thermodynamically favorable surfaces for oxygen and NO adsorption on PdO(101); (a) with 0.25 ML coverage of oxygen, (b) with 0.25 ML coverage of NO, (c) with 0.5 ML coverage of NO, and (d) with 1 ML coverage of NO.

"oxygen poor limit" is the same for both cases. However, for CO_2 molecule (from our calculations $E_{CO_2}^{bind}=-17.41$ eV, $E_{CO}^{bind}=-11.22$ eV) the quantity $E_{CO_2}^{bind}-E_{CO}^{bind}-\frac{1}{2}E_{O_2}^{bind}=-3.38$ eV, and for NO_2: $E_{NO_2}^{bind}-E_{NO}^{bind}-\frac{1}{2}E_{O_2}^{bind}=-1.2$ eV. From this simple analysis, it is obvious that CO_2 is much more stable than NO_2. Therefore, a low chemical potential of CO is needed to destroy bulk PdO, while in the case of NO oxidation a much higher pressure of NO is needed to decompose bulk PdO. In CO oxidation, this result leads to a constraint such that the bulk oxide is stable when $\Delta\mu_{CO}-\Delta\mu_O \leq -1.8$ eV.

It is important to remember that we have only considered thermodynamics in this analysis. Lundgren *et al.*[47] have studied the kinetics of PdO oxidation using surface x-ray diffraction (SXRD) and found that for $T<600$ K, even up to ambient pressures, the surface oxide grown on Pd(100) will remain the most stable structure although the bulk oxide is predicted to form. Their result implies that a kinetic hindrance to the formation of the bulk oxide must exist. Given the massive restructuring required, it is not surprising that bulk oxide formation is a highly activated process.

In the particular circumstances surrounding NSR catalysis, the atmosphere is cycled between oxidizing and reducing conditions.[3] In the oxidation mode, the partial pressures of oxygen and NO reach 1 bar and 1 mbar, respectively, whereas during the reduction cycle the partial pressure of oxygen vanishes (although nitrogen oxides are released from the barium nitrates). It should be noted that temperatures can vary greatly across the reactor system and that the overall operating conditions can vary widely from ambient temperature during the cold startup to 450 °C in gasoline engine based NSR systems.[2] Of course, changing the temperature will not change which phases exists on our diagram but will merely serve to shift the pressure which results in the same chemical potential.[11] We find that the pristine PdO surface is likely to be favored under typical lean burn conditions in NSR even when including the possibility for NO or O_2 adsorption on this surface. However, it is not known if this surface is active for NO oxidation (although analogous results for CO oxidation indicate this is possible[42]). On the other hand, it is interesting to note that by applying a similar thermodynamic analysis to the reduction in the PdO surface with a reductant such as ethylene, almost any pressure of the reductant is sufficient to convert the oxide back to the metal. Therefore, the improved activity of the Pd catalyst may be explained by the fact that oxide formation is slow compared to the oxidation cycle time. In addition, the presence of the reductant returns the system to the pristine metal rapidly during the reduction portion of the NSR cycle. In fact, given the complexity of the dynamics of NSR, it precludes simple analysis here but, it may be possible that equilibrium is never reached at any point throughout the cycle. So while the formation of the PdO(101) surface (above a PdO bulk) may be favored over both Pd(111) and Pd(100) thermodynamically, kinetics may control how these surfaces form oxides (and how those oxides decompose) resulting in structural differences. Indeed, for the case of Pt, significant differences are observed between structures.[6] Finally, concentrations of the reactants vary considerably across the reactor such that a single description of the catalytic surface is improbable. Nevertheless, on the basis of these results it may be instructive to measure the formation of oxides under NSR operating conditions and in addition, if kinetics rather than thermodynamics ultimately controls the catalyst surface, other materials which oxidize more easily than Pt (i.e., Pd) could be viable options for NSR systems.

IV. CONCLUSIONS

Ab initio thermodynamics has been used to analyze the stable surface structures of Pd(100) and Pd(111) under NO oxidation conditions. Formation of NO_2 in the gas phase and readsorption to the surface were neglected, as a first approximation, so the effect of the surrounding gas phase on the surface structure and composition is modeled through contact with independent reservoirs representing the reactants. Many possible structures with O and NO adsorbed on Pd(100) and Pd(111) and surface oxides have been considered in order to construct phase diagrams. At first glance, from the phase diagrams we can conclude that in typical NSR catalyst working conditions bulk oxide will be formed. However, kinetic limitations may exist such that its formation is slow compared to the cycling of the NSR system. In addition the presence of reductants during the rich portion of the NSR cycle may return the surface to the pristine metal resulting in transient conditions that prevent a single description of the catalytic surface.

ACKNOWLEDGMENTS

We gratefully acknowledge funding for this work from the National Science Foundation (CBET Grant No. 0730937). We would also like to acknowledge Jason Weaver and Aravind Asthagiri for their input on this work.

[1] N. Takahashi, H. Shinjoh, T. Iijima, T. Suzuki, K. Yamazaki, K. Yokota, H. Suzuki, N. Miyoshi, S. Matsumoto, T. Tanizawa, T. Tanaka, S. Tateishi, and K. Kasahara, Catal. Today **27**, 63 (1996).
[2] S. Matsumoto, Catal. Today **29**, 43 (1996).
[3] S. Matsumoto, CATTECH **4**, 102 (2000).
[4] Y. Su, K. S. Kabin, M. P. Harold, and M. D. Amiridis, Appl. Catal., B **71**, 207 (2007).
[5] S. Ovesson, B. I. Lundqvist, W. F. Schneider, and A. Bogicevic, Phys. Rev. B **71**, 115406 (2005).
[6] A. D. Smeltz, R. B. Getman, W. F. Schneider, and F. H. Ribeiro, Catal. Today **136**, 84 (2008).
[7] B. L. M. Hendriksen, S. C. Bobaru, and J. W. M. Frenken, Catal. Today **105**, 234 (2005).
[8] B. L. M. Hendriksen, S. C. Bobaru, and J. W. M. Frenken, Surf. Sci. **552**, 229 (2004).
[9] K. Reuter and M. Scheffler, Phys. Rev. Lett. **90**, 046103 (2003).
[10] K. Reuter and M. Scheffler, Phys. Rev. B **68**, 045407 (2003).
[11] J. Rogal, K. Reuter, and M. Scheffler, Phys. Rev. B **75**, 205433 (2007).
[12] K. Reuter and M. Scheffler, Appl. Phys. A: Mater. Sci. Process. **78**, 793 (2004).
[13] J. Rogal, K. Reuter, and M. Scheffler, Phys. Rev. Lett. **98**, 046101 (2007).
[14] J. Rogal, K. Reuter, and M. Scheffler, Phys. Rev. B **69**, 075421 (2004).
[15] M. Todorova, K. Reuter, and M. Scheffler, Phys. Rev. B **71**, 195403 (2005).
[16] M. Todorova, K. Reuter, and M. Scheffler, J. Phys. Chem. B **108**, 14477 (2004).
[17] M. S. Chen, Y. Cal, Z. Yan, K. K. Gath, S. Axnanda, and D. W. Goodman, Surf. Sci. **601**, 5326 (2007).
[18] G. Kresse and J. Furthmuller, Phys. Rev. B **54**, 11169 (1996).
[19] G. Kresse and J. Furthmuller, Comput. Mater. Sci. **6**, 15 (1996).
[20] D. Vanderbilt, Phys. Rev. B **41**, 7892 (1990).
[21] J. P. Perdew and Y. Wang, Phys. Rev. B **45**, 13244 (1992).
[22] H. J. Monkhorst and J. D. Pack, Phys. Rev. B **13**, 5188 (1976).
[23] M. Todorova, E. Lundgren, V. Blum, A. Mikkelsen, S. Gray, J. Gustafson, M. Borg, J. Rogal, K. Reuter, J. N. Andersen, and M. Scheffler, Surf. Sci. **541**, 101 (2003).
[24] M. Saidy, O. L. Warren, P. A. Thiel, and K. A. R. Mitchell, Surf. Sci. **494**, L799 (2001).
[25] H. Gabasch, W. Unterberger, K. Hayek, B. Klotzer, G. Kresse, C. Klein, M. Schmid, and P. Varga, Surf. Sci. **600**, 205 (2006).
[26] K. Reuter and M. Scheffler, Phys. Rev. B **65**, 035406 (2001).
[27] X. G. Wang, A. Chaka, and M. Scheffler, Phys. Rev. Lett. **84**, 3650 (2000).
[28] X. G. Wang, W. Weiss, S. K. Shaikhutdinov, M. Ritter, M. Petersen, F. Wagner, R. Schlogl, and M. Scheffler, Phys. Rev. Lett. **81**, 1038 (1998).
[29] M. W. Chase, Jr., NIST-JANAF Thermochemical Tables, 4th ed., J. Phys. Chem. Ref. Data Monogr. **9**, 1 (1998).
[30] G. Zheng and E. I. Altman, Surf. Sci. **504**, 253 (2002).
[31] E. M. Stuve, R. J. Madix, and C. R. Brundle, Surf. Sci. **146**, 155 (1984).
[32] M. Todorova, K. Reuter, and M. Scheffler, Phys. Rev. B **71**, 195403 (2005).
[33] Y. S. Zhang, V. Blum, and K. Reuter, Phys. Rev. B **75**, 235406 (2007).
[34] A. Steltenpohl and N. Memmel, Surf. Sci. **443**, 13 (1999).
[35] A. Eichler, F. Mittendorfer, and J. Hafner, Phys. Rev. B **62**, 4744 (2000).
[36] A. J. Jaworowski, R. Asmundsson, P. Uvdal, and A. Sandell, Surf. Sci. **501**, 74 (2002).
[37] I. Nakamura, T. Fujitani, and H. Hamada, Surf. Sci. **514**, 409 (2002).
[38] M. Gajdoš, J. Hafner, and A. Eichler, J. Phys.: Condens. Matter **18**, 13 (2006).
[39] K. Højrup Hansen, Ž. Šljivančanin, B. Hammer, E. Lægsgaard, F. Besenbacher, and I. Stensgaard, Surf. Sci. **496**, 1 (2002).
[40] R. T. Vang, J. G. Wang, J. Knudsen, J. Schnadt, E. Laegsgaard, I. Stensgaard, and F. Besenbacher, J. Phys. Chem. B **109**, 14262 (2005).
[41] P. J. Chen and D. W. Goodman, Surf. Sci. **297**, L93 (1993).
[42] J. A. Hinojosa, Jr., H. H. Kan, and J. F. Weaver, J. Phys. Chem. C **112**, 8324 (2008).
[43] R. B. Getman, Y. Xu, and W. F. Schneider, J. Phys. Chem. C **112**, 9559 (2008).
[44] M. W. Chase, C. A. Davies, J. R. Downey, D. J. Frurip, R. A. Mcdonald, and A. N. Syverud, J. Phys. Chem. Ref. Data **14**, 1 (1985).
[45] A. Hellman, I. Panas, and H. Gronbeck, J. Chem. Phys. **128**, 104704 (2008).
[46] H. H. Kan and J. F. Weaver, Surf. Sci. **602**, L53 (2008).
[47] E. Lundgren, J. Gustafson, A. Mikkelsen, J. N. Andersen, A. Stierle, H. Dosch, M. Todorova, J. Rogal, K. Reuter, and M. Scheffler, Phys. Rev. Lett. **92**, 046101 (2004).